799. Hopf bifurcation and stability analysis of flexible rotor-bearing system

Ji Feng[1], Yang Jinfu[2], Yuan Xiaoyang[3]
[1, 3]Key Laboratory of Education Ministry for Modern Design and Rotor-Bearing System
Xi'an Jiaotong University, Xi'an, China, 710049
[2]Institute of Engineering Thermophysics, Chinese Academy of Sciences, Beijing, 100190
E-mail: [1]*jifengxjtu@126.com*, [3]*xyyuan@mail.xjtu.edu.cn*

Abstract. Analytical model of a long bearing was used to study the self-excited vibration of a single disc flexible rotor-bearing system on sliding bearing support. A shooting method was applied to track and acquire periodic solution of flexible rotor system after the Hopf bifurcation. Stability of periodic solution was analyzed on the basis of Floquet theory. Gas film eddying, oscillation and other nonlinear features were considered. High-speed air hybrid bearing test-bed was used to verify gas film oscillation arising from coupling between natural frequency and gas film eddying frequency. The "bounded" nature of chaotic vibration and the process of rubbing caused by instability of air film were observed. Finally, a distinguishing criterion named "practical stability" was provided.

Keywords: nonlinear, stability, chaos, air whip.

1. Introduction

Generally speaking, linear vibration theory and methods are adopted in traditional rotor dynamics research. When solving the actual engineering problems, reasonable linearization can apparently reduce the workload of analysis and calculation, however, the actual linear prediction results of rotor-bearing system cannot comprehensively reflect the motion mechanism of bearing oil film. As the rotating speed of machinery increases continuously, there is oil film force, sealing force, air flow excitation force and other many strong nonlinear excitation sources in high-speed rotor-bearing system, causing various nonlinearities in the rotor system. With sufficient facts, linear vibration theory has been unable to properly solve the problem of nonlinear vibration. For the rotor-bearing system containing a large number of strong nonlinear factors, the research on nonlinear dynamic analysis methods is required to make the system meet the actual engineering situation to a higher degree.

Oil film force model for high-speed low-duty rotor bearing that can explain oil film instability mechanism was raised by Muszynska [1]. This model offered the relationship between cross stiffness of oil film caused instability and average velocity factor, rotating speed and external damping, however, the coefficients in model should be determined through experiment, and certain limitation existed in the application. Nonlinear dynamic oil film force analytical model in the assumption of short bearing was put forward by Capone [2]. In short bearing assumption, circumferential pressure gradient was ignored, and analytical model of corrected short cylinder bush bearing nonlinear oil film force was obtained. Meng [3] studied sliding bearing nonlinear oil film force database, attained nonlinear oil film force of the same category of bearings on different centric positions and at different velocity through calculation, and stored in numerical documents according to certain order to form oil film force database. Nonlinear oil film force can be calculated only by retrieving interpolation in the database, providing a convenient and efficient method. In high-speed rotor bearing system, high rotating speed will induce exciting vibration sources of several frequencies, such as foundation vibration, oil film eddying, and all of these will increase system vibration and result in rubbing among stationary and moving dynamic and static components. Adiletta [4, 5] performed a relatively thoirough theoretical analysis and experimental research for one rigid rotor bearing system, compared experiment results with theoretical analysis results, and discovered that considerable

parts fit, but part of results had tremendous differences. Su [6] implemented numerical analysis for dynamic stability of hybrid air bearing with many rows of micropores, calculated bearing's rigidity and damping coefficient with method of perturbation, and determined rotating speed of rotor instability. Leonard [7] conducted dynamic pressure air bearing test, studied dynamic coefficient and eddying mechanism, and predicted the starting point of instability.

This paper is based on theoretical and experimental research and starts with nonlinear oil film force equation and system's periodic solution solving method to analyze gas film eddying and oscillation as well as other nonlinear features of instability phenomenon. High-speed air hybrid bearing test-bed was used to verify gas film oscillation arising from coupling between natural frequency and gas film eddying frequency. "Bounded" nature of chaotic vibration was found out as well as the process of rubbing caused by instability of air film. In addition, one kind of distinguishing criterion of "practical stability" was provided.

2. Dynamic equations of rotor-sliding bearing system

The mechanical model of a flexible rotor is shown in Fig. 1(a). The reference coordinate system of bearing is shown in Fig. 1(b).
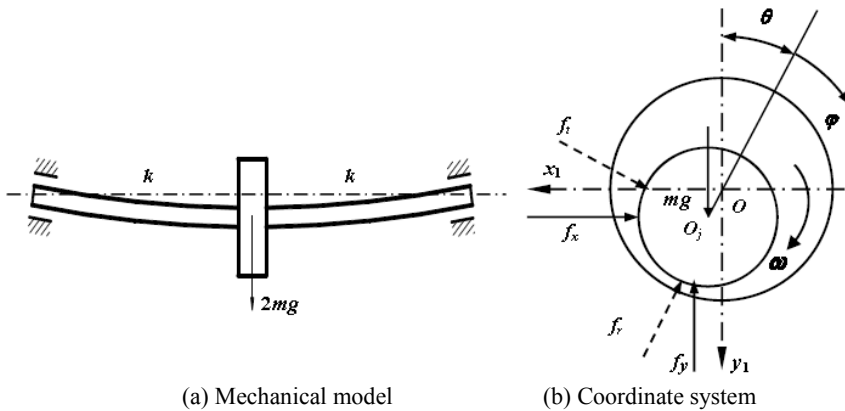
(a) Mechanical model (b) Coordinate system
Fig. 1. Flexible rotor-bearing system

Where ω is rotor angular velocity, f_x and f_y are oil film force components of sliding bearings, θ is attitude angle, O is geometric center of bearing, O_j is geometric center of journal, g is acceleration of gravity. The motion equation of journal center O_j is:

$$\begin{cases} m_1\ddot{x}_1 + k(x_1 - x_2) + f_x = 0 \\ m_1\ddot{y}_2 + k(y_1 - y_2) + f_y - m_1 g = 0 \end{cases} \tag{1}$$

The motion equation of disc O_i is:

$$\begin{cases} m_2\ddot{x}_2 + 2k(x_2 - x_1) = 0 \\ m_2\ddot{y}_2 + 2k(y_2 - y_1) - m_2 g = 0 \end{cases} \tag{2}$$

where m_1 and m_2 are quality of rotor and disc, $2m$ is total mass. x_1, y_1, x_2 and y_2 are displacement component of x and y direction for rotor and disc. The infinite length bearing model is chosen in this paper.

724

Parameter $\sigma = \dfrac{\mu \omega L R^3}{W c^2}$, where c is radius clearance of bearing, bearing load is $W = mg$, σ is the reciprocal of dimensionless load, namely Somerfield number. The dimensionless transform is introduced as follows:

$$X_i = \frac{x_i}{c}, Y_i = \frac{y_i}{c}, \quad F_x = \frac{f_x}{\sigma W}, F_y = \frac{f_y}{\sigma W}, \quad M_i = \frac{m_i}{m}, K = \frac{k \cdot c}{mg}, \quad \tau = \omega t, \overline{\omega} = \omega \sqrt{\frac{c}{g}}.$$

The dimensionless form of motion equation is:

$$\begin{cases} \overline{\omega}^2 M_1 X_1'' + K(X_1 - X_2) + \sigma F_x = 0 \\ \overline{\omega}^2 M_1 Y_1'' + K(Y_1 - Y_2) + \sigma F_y - M_1 = 0 \\ \overline{\omega}^2 M_2 X_2'' + 2K(X_2 - X_1) = 0 \\ \overline{\omega}^2 M_2 Y_2'' + 2K(Y_2 - Y_1) - M_2 = 0 \end{cases} \tag{3}$$

The state variables are introduced:

$$\mu = \{\mu_1, \mu_2, \mu_3, \mu_4, \mu_5, \mu_6, \mu_7, \mu_8\} = \{X_1, Y_1, X_1', Y_1', X_2, Y_2, X_2', Y_2'\}$$

The motion equation of system state space is obtained:

$$\begin{cases} u_1' = u_3 \\ u_2' = u_4 \\ u_3' = (K(u_5 - u_1) - \sigma F_x)/(\overline{\omega}^2 M_1) \\ u_4' = (K(u_6 - u_2) - \sigma F_y)/(\overline{\omega}^2 M_1) \\ u_5' = u_7 \\ u_6' = u_8 \\ u_7' = (2K(u_1 - u_5) - \sigma F_x)/(\overline{\omega}^2 M_1) \\ u_8' = (2K(u_2 - u_6) - \sigma F_y)/(\overline{\omega}^2 M_1) \end{cases} \tag{4}$$

where F_x and F_y are dimensionless liquid-film force of bearing, ε is eccentricity:

$$\begin{cases} F_r = 6\{(1 - 2\theta')\dfrac{2\varepsilon^2}{(2 + \varepsilon^2)(1 - \varepsilon^2)} + \dfrac{\varepsilon'[\pi^2(2 + \varepsilon^2) - 16]}{\pi(2 + \varepsilon^2)(1 - \varepsilon^2)^{3/2}}\} \\ F_t = -6\{(1 - 2\theta')\dfrac{\pi\varepsilon}{(2 + \varepsilon^2)(1 - \varepsilon^2)^{1/2}} + \dfrac{4\varepsilon\varepsilon'}{(2 + \varepsilon^2)(1 - \varepsilon^2)}\} \end{cases} \tag{5}$$

$$\begin{cases} F_x = F_t \cos\theta + F_r \sin\theta \\ F_y = -F_t \sin\theta + F_r \cos\theta \end{cases} \tag{6}$$

3. Periodic solution and stability discrimination

3. 1 Calculation method of periodic solution

The periodic solutions of the system (4) needs to meet the following conditions:

$$u(t) = u(t + T) \tag{7}$$

where T is period. Solving periodic solutions of equality (7) is more time-consuming by direct integration method and cannot detect the unstable solution. It is very inconvenient for the study the bifurcation behavior. Periodic solutions are obtained using the shooting method in this paper. So the periodic solutions problem for equation (4) is transformed into fixed point of Poincare map, that is:

$$G(u) = u - P(u) = 0 \tag{8}$$

Equality (8) is solved using the method of iterative Newton-Raphson. The results can be expressed as:

$$u_{k+1} = u_k - [G_{\boldsymbol{u}}{}'(u_k)]^{-1} \cdot G(u_k) \tag{9}$$

In which $G_u'(u_k)$ is the Jacobin matrix of G at given point. The partial derivative of equality (9) is:

$$\frac{d}{dt}\left(\frac{\partial u}{\partial u_0}\right) = F_u'(t, u)\left(\frac{\partial u}{\partial u_0}\right) \tag{10}$$

Assumption u_0 is the initial value and $u_0^{(1)}$ is the next Poincare map point, namely $u_0^{(1)} = P(u_0)$, the following result can be achieved:

$$\frac{\partial u}{\partial u} = I, \; \frac{\partial u_0^{(1)}}{\partial u_0} = P_u'(u_0) \tag{11}$$

The method mentioned above including shooting method and Newton iteration method, which has convergence properties of Newton method, can achieve higher efficiency for solving periodic solutions.

The Poincare map fixed point u^* and Jacobin matrix $P_u'(u^*)$ of system periodic solution can be obtained through Newton shooting method. The eigenvalue of $P_u'(u^*)$ is called Floquet multiplier. Perturbation equation of system periodic solution is a differential equation in terms of periodic coefficient variable. The stability of periodic solution can be judged by stability rules. The periodic solution is instability when the maxima mode of Floquet multiplier is larger than 1.

3. 2 Numerical calculation

A flexible single disc symmetric rotor is considered as a research object: rotor diameter 50 mm, span 475 mm, density 7800 kg·m^{-1}, modulus of elasticity 2.1×10^{11} N·m^{-1}, total mass 12 kg, air hybrid bearing diameter 50 mm, width 38 mm, diametric clearance 0.1 mm, clearance ratio 2‰.

Periodic unbalance response of system was tracked using shooting method tracking system and a series of system's periodic solutions at different rotating speed was obtained. Fig. 2 shows amplitude - rotating speed curve at the disc in the middle of rotor under continuously changed rotating speed. Maximum amplitude at horizontal direction is 95.4 μm, and the corresponding

rotating speed is 11232 r·min^{-1}. Maximum amplitude at vertical direction is 69.4 μm, and the corresponding rotating speed is 11808 r·min^{-1}.
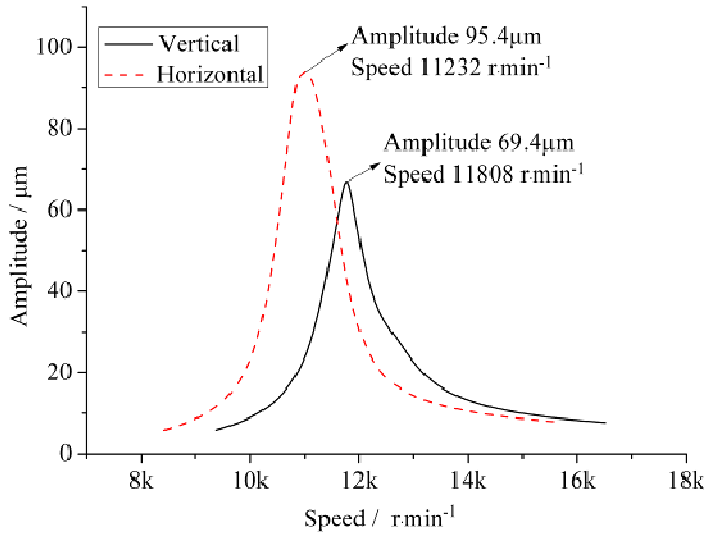

Fig. 2. Amplitude - rotating speed curve

Fig. 3 illustrates the time domain oscillogram and frequency spectrogram of disc vibration at vertical direction when the rotating speed is 15694 r·min^{-1} after bifurcation. "Beating" phenomenon can be observed from time domain oscillogram, and frequency spectrogram reveals that the vibration contained power frequency as well as bigger low frequency components. Real part of Floquet multipliers were changed from negative to positive, synchronous periodic solution lost stability and the system made quasi-periodic motion.


(a) Time domain oscillogram   (b) Spectrogram
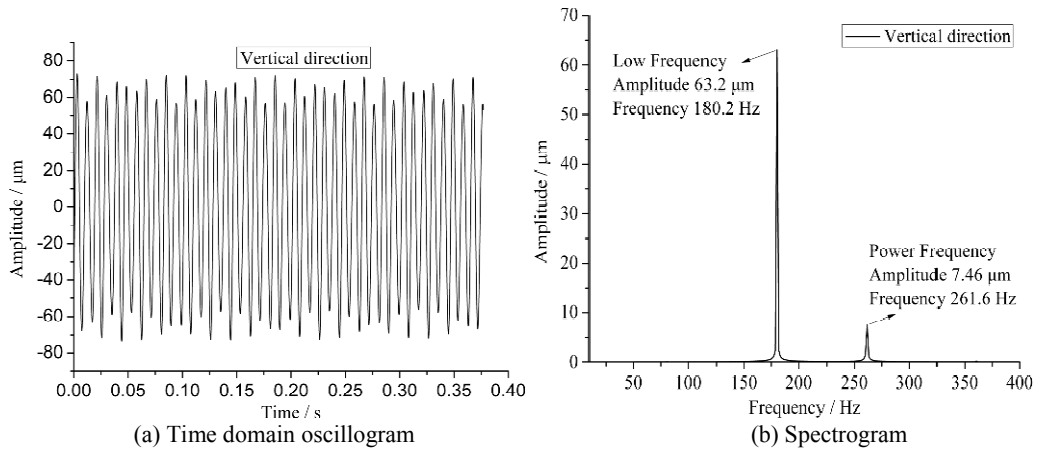
Fig. 3. Oscillogram and spectrogram of vibration at vertical direction

Fig. 4 presents axis orbit at disc. Fig. 5 illustrates the system's motion bifurcation diagram, the system's synchronous periodic solution path is projected into one point on the coordinates of state space, after bifurcation, the path will be spread on one ring surface, and the project on the coordinates will form the belt with certain width.

727
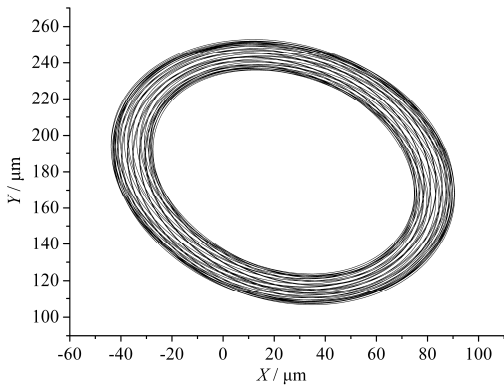
Fig. 4. Axis orbit
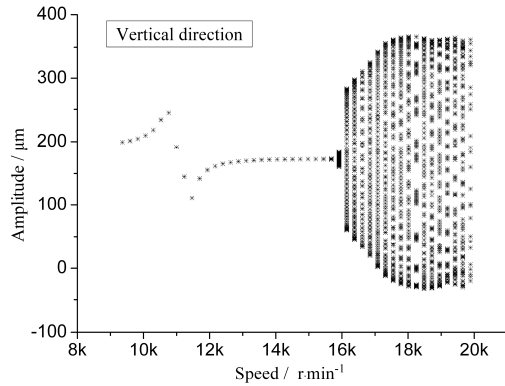
Fig. 5. Bifurcation diagram

In this calculation example, unbalanced eccentricity had certain impact on system stability. As unbalanced eccentricity increased, rotating speed of system instability would increase. Rotating speed of instability with eccentricity is bigger than that of the balanced system, indicating that unbalanced eccentricity would sometimes increase system stability, and the literature [8] proves this as well.

4. Experimental study of nonlinear vibration performance for high-speed air hybrid bearing

4. 1 Air hybrid bearing test-bed

In this section, air hybrid bearing was utilized to conduct experimental research of bearing vibration performance in fast vibration process, including bearing eddying and oscillation as well as other nonlinear dynamic behavior induced during high-speed operation.

Test-bed consists of gas compressor, expander and air bearing - rotor system. Lubrication medium is dry and clean air, which is compressed with a compressor to make the pressure higher and will be entered into turbine air inlet after being expanded via expander, and then through means of pressure control to realize high rotating speed, fast variation and other processes. Fig. 6 provides the structural diagram of the test-bed, in which No. 1-8 are volute, compressor impeller, rotor, air bearing, thrust disc, rubber ring, expander impeller and case, respectively.
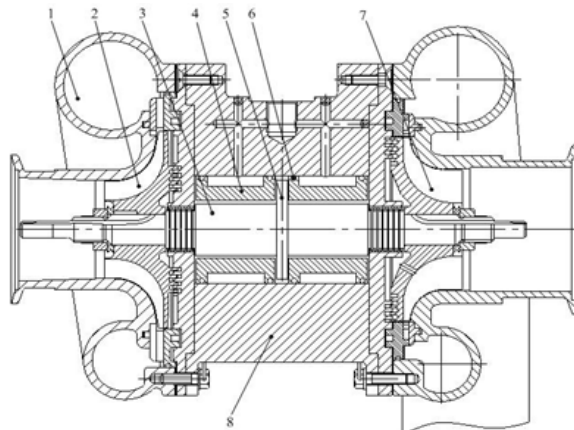

Fig. 6. Structural diagram of a test-bed

728

The internal surface of air hybrid bearing bush has a herringbone groove, in which four rows of throttling holes are under axial distribution, and 20 holes are evenly distributed at each circumferential direction, and the tangential air feeding method that is opposite to rotor steering is adopted. Bearing material is nonmetal graphite alloy, which has excellent dry friction, self-lubrication performance and small hardness. The test indicated that this material had excellent dry friction and self-lubricating performance and small hardness for easy processing. Fig. 7 provides the structural diagram of air hybrid bearing. Table 1 lists main structural parameters of the test-bed and air hybrid bearing.
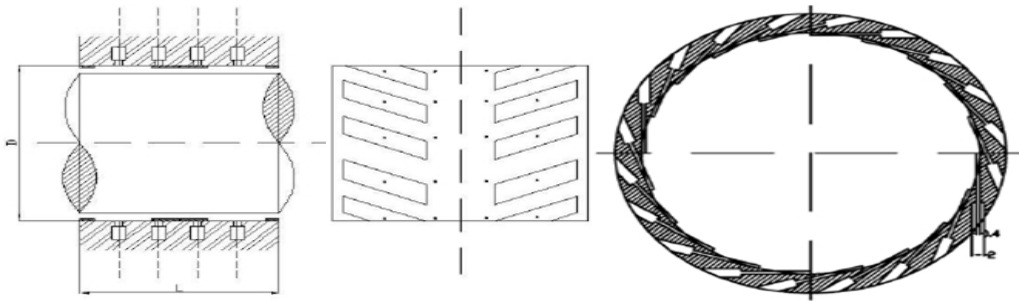

Fig. 7. The structural diagram of air hybrid bearing

Table 1. Structural parameters of test-bed and air hybrid bearing

Test-bed		Air hybrid bearing	
Rotor diameter / mm	50	Width / mm	38
Rotor length / mm	590	Inner diameter / mm	50
Thrust plate diameter / mm	94	Outer diameter / mm	64
Span / mm	475	Diametric clearance / mm	0.1
Rotor quality / kg	12	Clearance ratio	2‰
Design speed / r·min^{-1}	60000	Aspect ratio	0.76

4. 2 Experimental analysis of non-linear vibration for air hybrid bearing

Rotor acceleration and deceleration curves visually describe rotor power frequency vibration situation in the whole experiment process. Rotor shaft vibration situation at horizontal direction is shown in Fig. 8 when the measuring point was in the middle of the rotor. Critical rotating speed during acceleration and deceleration was 12940 r·min^{-1} and 12106 r·min^{-1} respectively, power frequency amplitude increased as rotating speed increased, and the amplitude was 72 μm in the critical point. Fig. 9 provides the bifurcation diagram of testing rotor acceleration process. It can be observed from the figure that system motion process is periodic motion (Region A) — chaotic motion (Region B) — motion in Period 2 (bifurcation, Region C) — chaotic motion (Region D).

Bifurcation diagram describes the path from stable operation in Period 1 to advent of chaotic instability during rotor acceleration. In the paper the method to obtain the bifurcation diagram is as follows: to obtain sample according to equal sampling points and take the rising edge of key phase signal at the beginning of sampling as zero reference. Each point on bifurcation diagram indicates the displacement of rising edge of key phase signal relative to zero reference, and number of sampling points at each rotating speed is equal to product between the set sampling frequency and sampling time. If displacement signal is stable, the amplitude at certain rotating speed on the bifurcation diagram is one constant value. If low frequency or high frequency component appears at certain rotating speed, there will be positive and negative amplitude on bifurcation diagram, i.e. period doubling or chaotic phenomenon will appear.

729
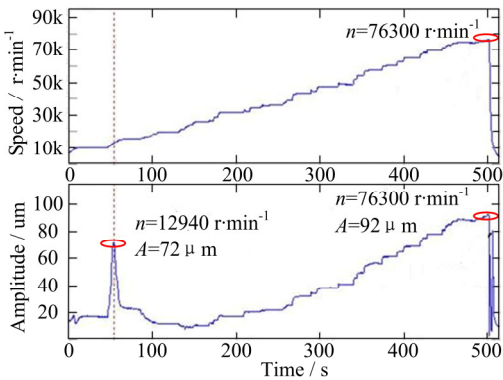
Fig. 8. Acceleration and deceleration curve
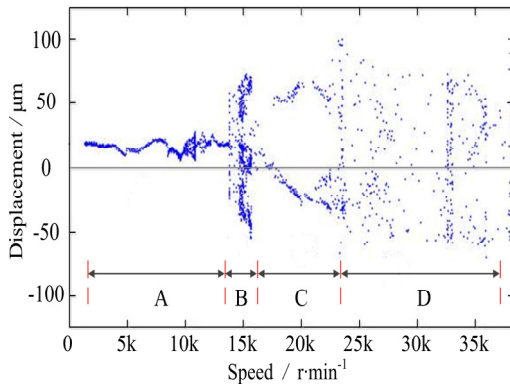
Fig. 9. Bifurcation diagram

The support rotor of air hybrid bearing exhibits vibration instability phenomenon under working conditions of critical rotating speed and rotating speed higher than 76000 r·min^{-1} during acceleration. But the nature of two times of instability was different, the former was power frequency vibration instability (Fig. 10(a)), rotor centric operating track was period motion, and frequency spectrogram only had one peak value of power frequency. The latter (Fig. 10(b)) was low frequency coupling vibration instability. According to frequency spectrogram, low frequency vibration amplitude nearly corresponds to power frequency vibration amplitude, and a quasi-periodic motion could be observed from axis orbit. The measured instability of the rotating speed in this acceleration experiment was about 76000 r·min^{-1}, but the design rotating speed of rotor design was 60000 r·min^{-1}, and the safety margin was 26.67 %, which could meet the design requirements of safety margin not less than 20 %.

(a) Power frequency instability

(b) Low frequency coupling instability
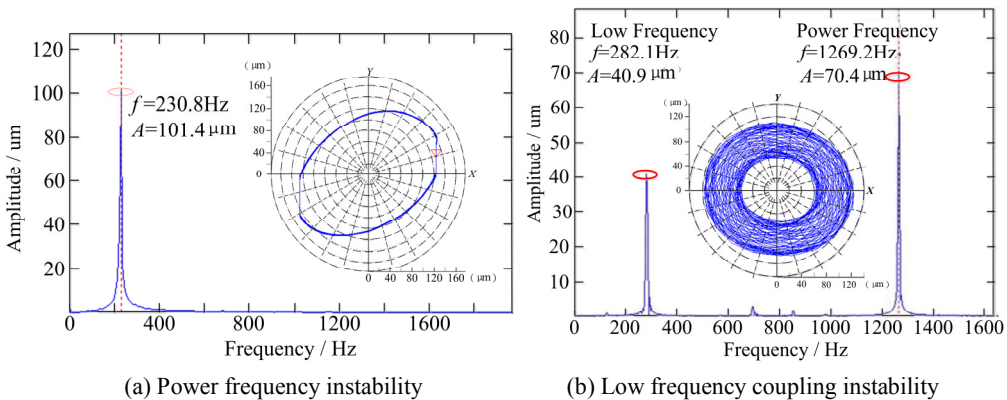
Fig. 10. Vibration instability

During rotor acceleration, low-frequency vibration coupled with rotor power frequency exists, and low-frequency vibration frequency and amplitude increased as rotating speed increased. The analysis demonstrated that during acceleration, increase of gas film dynamic pressure in the bearing led to increase of dynamic rigidity of gas film, thus resulting in the increase of shaft natural frequency. According to axis orbit diagram, rubbing features in the process of low frequency coupling resonance can be obtained. However, test data revealed that hybrid bearing experienced load bearing failure at 76154 r·min^{-1}, resulting in dynamic and static rubbing of bearing. In the meantime, low-frequency vibration frequency rose from 285.7 Hz to 296.2 Hz, and amplitude increased from 35.9 μm to 67.8 μm. The above phenomena proved

730

that, when rubbing between axial vibration and bush became more pronounced, shaft exhibits varied rigidity support character, that is, overall support rigidity of bush, foundation and gas film was changed into the higher rigidity of bush and foundation. Because the previous rigidity is very small, rubbing process increased support rigidity and shaft natural frequency. Most of literature [9, 10] adopted Poincare mapping to provide bifurcation diagram taking rotating speed as parameters in different non-equilibrium volume through calculation, and this section demonstrated the known bifurcation and hybrid phenomena by means of experiment.

Fig. 11 illustrates frequency spectrogram and axis orbit features when rubbing between rotor and bearing at turbine side. Fig. 10(b) provides a quasi-periodic motion before the rotor is rubbed. Low frequency with frequency 282.1 Hz and amplitude 40.9 μm may be observed from frequency spectrogram. Gas film instability component force corresponding to this low frequency caused chaotic motion of rotor. It can be clearly observed in Fig. 11(a) that axis orbit during full annular rubbing vibration could not be further diffused due to the constraint of bearing interval, therefore straight line appeared outside of axis orbit. During rubbing, low-frequency vibration amplitude was 71.6 μm, energy was released in the rubbing process, and vibration amplitude of power frequency as well as low frequency decreased. Fig. 11(b) presents vibration frequency spectrogram when rotor is away from rubbing. Linear boundary in axis orbit started to decrease until axis orbit became irregular circle again, but low frequency still existed, so axis orbit indicates that the rotor was still quasi-periodic motion.


(a) Full annular rub   (b) Away from rubbing
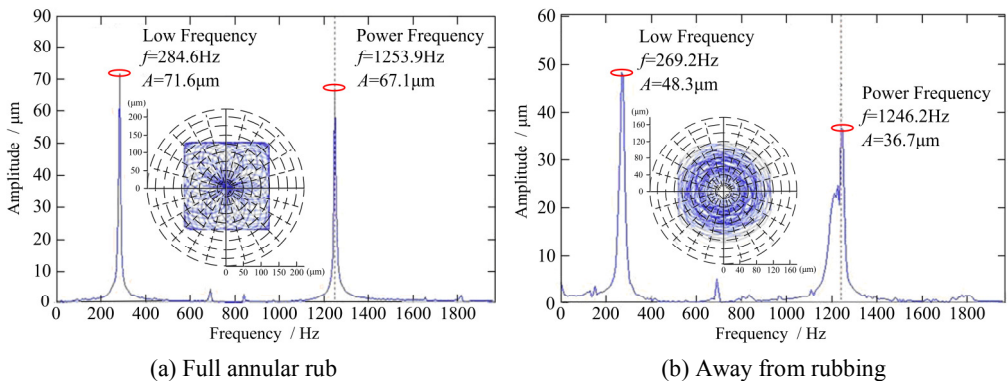
Fig. 11. Spectrogram and axis orbit when rubbing between rotor and bearing

As far as the actual engineering, rotor system stability criterion does not have the uniform standard. Lyapunov's stability criterion or Floquet theory cannot be used to judge about the stability of complicated shafting in actual application, although they have complete theoretical system. From the angle of engineering, no matter half-speed eddying or liquid film oscillation appears, as long as the amplitude does not exceed the maximum safety limit restricted by bearing interval, the system is always stable in the actual engineering meaning. If the eccentricity and variation velocity can be controlled, obvious restraint vibration effect will be exerted, and the system will still be considered as stable. It is possible to use "whether the journal's liquid film bearing capacity exceeds external load under the operation of maximum allowable eccentricity" as the condition for effectively judging about engineering stability, which is the easiest to implement.

5. Conclusions

1) An infinite long bearing model with analytical solutions was applied to establish dynamic model of unbalanced flexible rotor-bearing system. A prolongation shooting method was used

to trace and solve system's periodic unbalance response and the solution stability and bifurcation character were analyzed.

2) The unbalanced eccentricity had certain impact on system stability. As unbalanced eccentricity increased, rotating speed of system instability would increase and rotating speed of instability with eccentricity was bigger than that of the balanced system indicating that unbalanced eccentricity would sometimes increase system stability.

3) Considering the existing rotor design in which attenuation ratio was used as the main indicator of system stability, it was possible and could be accomplished with the least effort to take "whether the journal's liquid film bearing capacity exceeds external load under the operation of maximum allowable eccentricity" as the condition for effectively judging about engineering stability.

Acknowledgements

References

[1] **Muszynska A.** Stability of whirl and whip in rotor-bearing systems. Journal of Sound and Vibration, Vol. 127, Issue 3, 1988, p. 49 – 64.

[2] **Capone G.** Descizione analitica del campo di forze fluidodinami – co nei cuscinetti cilindrici lubrifieati. L'Energia Elettrica, Vol. 68, Issue 3, 1991, p. 105 – 110.

[3] **Meng Z. Q., Xu H., Zhu J.** A database method of nonlinear oil film force based on Poincare transformation. Tribology, Vol. 21, Issue 3, 2001, p. 223 – 227.

[4] **Adiletta G., Guido A. R., Rossi C.** Nonlinear dynamics of a rigid unbalanced rotor in journal bearing, Part I: Theoretical analysis. Nonlinear Dynamics, Vol. 14, Issue 4, 1997, p. 57 – 87.

[5] **Adiletta G., Guido A. R., Rossi C.** Nonlinear dynamics of a rigid unbalanced rotor in journal bearings, Part II: Experimental analysis. Nonlinear Dynamics, Vol. 14, Issue 4, 1997, p. 157 – 189.

[6] **Su J. C. T., Lie K. N.** Rotor dynamic instability analysis on hybrid air journal bearings. Tribology International, Vol. 39, Issue 12, 2006, p. 238 – 248.

[7] **Leonard R., Rowe W. B.** Dynamic force coefficients and the mechanism of instability in hydrostatic journal bearings. Wear, Vol. 23, Issue 2, 1973, p. 277 – 282.

[8] **Li J. G.** The stability nonlinear vibrations and the oil unstable control for a bearing－rotor system. Mechanical Engineering, Xi'an Jiaotong University, Xi'an, 1992.

[9] **Zheng T. S., Hasebe N.** Calculation of equilibrium position and dynamic coefficients of a journal bearing using free boundary theory. Journal of Tribology - Transactions of the ASME, Vol. 122, Issue 4, 2000, p. 616 – 621.

[10] **Osborne D. A., San Andres L.** Experimental response of simple gas hybrid bearings for oil-free turbomachinery. Journal of Engineering for Gas Turbines and Power - Transactions of the ASME, Vol. 128, Issue 4, 2006, p. 626 – 633.